Nuclear and magnetic structural properties of Ba_2FeMoO_6

O. Chmaissem, B. Dabrowski, and S. Kolesnik
Department of Physics, Northern Illinois University, DeKalb, Illinois 60115, USA
and Materials Science Division, Argonne National Laboratory, Argonne, Illinois 60439, USA

S. Short and J. D. Jorgensen
Materials Science Division, Argonne National Laboratory, Argonne, Illinois 60439, USA
(Received 7 January 2005; published 24 May 2005)

Using neutron powder diffraction, we have investigated the structure of Ba_2FeMoO_6 at temperatures between 10 and 490 K. The structure of Ba_2FeMoO_6 is cubic $Fm\bar{3}m$ and tetragonal $I4/mmm$ above and below T_C, respectively. The tetragonal structure exhibits a c axis that is only slightly longer than the basal a parameter. A structural distortion from the cubic symmetry is required by the ferromagnetic alignment of Fe and Mo spins along a specific axis. The ferrimagnetic structure of the Fe and Mo sublattices is well described in the magnetic $I4/mm'm'$ space group. At 10 K, the FM moments for Fe and Mo refine to $\sim 4.1(1)\ \mu_B$ and $\sim -0.58(1)\ \mu_B$, respectively, with a total ferrimagnetic moment of $\sim 3.52\ \mu_B$, in good agreement with the magnetization results and the high spin state of the Fe electrons. The lower than expected ferrimagnetic moment is attributed to the presence of Fe and Mo in multiple oxidation states and possible site vacancies. Bond-valence-sum calculations reveal the presence of significant strains in this system.

DOI: 10.1103/PhysRevB.71.174421 PACS number(s): 61.12.−q, 75.50.Gg

INTRODUCTION

The recent observation of room-temperature tunneling magnetoresistance in half-metallic A_2FeMoO_6 (A = Ca, Sr, Ba) double perovskites,[1,2] and their importance to the emerging field of spintronics has led to considerable effort dedicated to detailed investigations of the physical and structural properties of these materials. In previous work, we showed that Sr_2FeMoO_6 crystallizes in cubic $Fm\bar{3}m$ and tetragonal $I4/m$ symmetries at temperatures above and below its Curie temperature (T_C), respectively.[3,4] The structure of its Ba_2FeMoO_6 counterpart, on the other hand, has frequently been described as being cubic at all temperatures above and below T_C, despite the material's ferrimagnetic properties that require it to have a lower symmetry. In this paper, we take into account the interaction between the nuclear lattice of the material and the ferrimagnetic ordering of its Fe and Mo spins to demonstrate that the structure of Ba_2FeMoO_6 is cubic $Fm\bar{3}m$ only at temperatures above T_C and tetragonal (pseudocubic) $I4/mmm$ in its ferrimagnetic state below T_C. The investigated material is ferrimagnetic below ~ 321 K with the magnitude of the Fe and Mo moments, reaching $\sim 4.1(1)\ \mu_B$ and $\sim -0.58(1)\ \mu_B$ at 10 K, respectively. Refinements of the tetragonal structure are stable and show that the slightly elongated c axis is the easy magnetic axis for spin alignment. Magnetization measurements, neutron powder diffraction, Mössbauer spectroscopy, x-ray absorption, and x-ray magnetic circular dichroism studies,[3,5–9] have demonstrated the antiferromagnetic coupling of the ferromagnetic Fe and Mo sublattices below their ordering temperature, (T_C) and revealed the presence of mixed oxidation states for Fe (2+/3+) and Mo (5+/6+) ions. Recent studies[10–13] have demonstrated that increasing the size of the A-site ion results in increasing the fractional amount of Fe^{2+}/Mo^{6+} pairs in the material. As such, the majority of Fe/Mo pairs would have oxidation states closer to 3+/5+ in Sr_2FeMoO_6 and to 2+/6+ in Ba_2FeMoO_6. Both valence combinations (Fe^{2+}—Mo^{6+} or Fe^{3+}—Mo^{5+}) would result in a saturated ferrimagnetic moment of 4 μ_B, however, the actual measured moment has always been observed to be considerably less than this value.

SYNTHESIS AND CHARACTERIZATION

Stoichiometric amounts of $BaCO_3$, Fe_2O_3, and MoO_3 were thoroughly ground and fired in air at 1000 °C for 2 days, resulting in gray precursors. The Ba_2FeMoO_6 double perovskite phase was obtained by heating the precursor in a flowing gas mixture of 0.5%–1% H_2/Ar, at a rate of 1.2 °C/min to 1150 °C for 2 h, followed by natural cooling of the material to room temperature. The final dark-blue dense pellets exhibited ferromagnetic properties at room temperature. Samples were characterized using room-temperature x-ray powder diffraction, neutron powder diffraction between 10 and 490 K, resistivity and magnetoresistive measurements (5–400 K), and dc magnetization (5–400 K) using a Quantum Design Physical Properties Measurement System-Model 6000.

Time-of-flight neutron powder diffraction data were collected on the special environment powder diffractometer (SEPD)[14] at the Intense Pulsed Neutron Source (IPNS). Diffraction data were acquired at several temperatures between 10 and 490 K using a closed-cycle helium refrigerator with heating capabilities. High-resolution backscattering data, from 0.5 to 4 Å, and medium-resolution data collected at 90° (data up to 10 Å), were used for the structural determination and analyzed using the Rietveld method and the General Structure Analysis System.[15] The medium-resolution bank was particularly useful for the magnetic refinements because it contained an additional magnetic peak (at

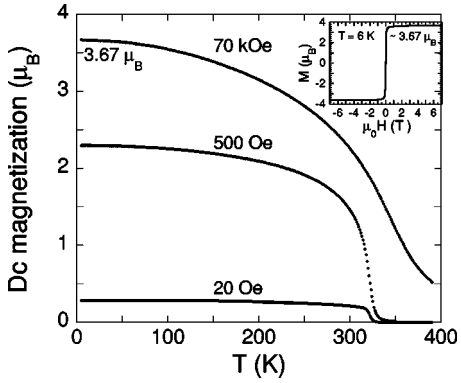

FIG. 1. Temperature-dependent dc magnetic susceptibility of Ba_2FeMoO_6. At 5 K, the magnetization saturates at 0.29, 2.29, and 3.67 μ_B under applied external fields of 20, 500, and 70 kOe, respectively. The low-field measurements at 20 Oe show that the ferromagnetic transition occurs at ~321 K (T_C) with an onset temperature near 327 K. Magnetization curve versus applied external magnetic field (up to 7 T) is shown in the inset. At 0.1 T, the spins are almost all aligned with a measured moment value of ~3.2 μ_B.

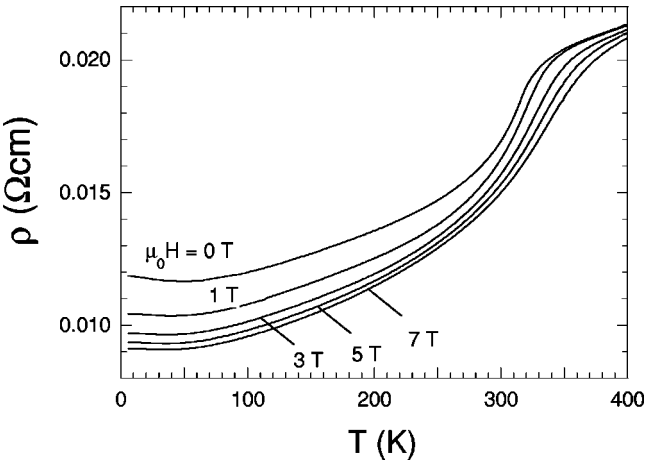

FIG. 2. Resistivity measurements as a function of temperature and applied magnetic fields are shown for our metallic Ba_2FeMoO_6 sample. The data clearly show a significant magnetoresistive response of ~30%–40% due to intergranular tunneling at temperatures below T_C and intragranular bulk effects around T_C.

~4.65 Å at 10 K). In the analysis, background parameters, peak-width variables, extinction, and absorption were refined, together with the lattice parameters, oxygen atomic positions, and isotropic and anisotropic temperature factors for the cations and oxygen, respectively.

RESULTS AND DISCUSSION

Magnetic and resistive properties

A ferrimagnetic transition temperature of ~321 K ($T_{C\ onset}$ ~327 K) is clearly observed in the temperature- and magnetic-field-dependent magnetization measurements of Ba_2FeMoO_6 (Fig. 1). As shown in the figure, at 6 K, a small field of about 1 kOe is large enough to nearly saturate the Fe and Mo spin alignment, thus yielding an effective moment of ~3.2 μ_B. At 70 kOe, the saturated moment reaches 3.67 μ_B (inset of Fig. 1).

Resistivity measurements as a function of temperature and applied magnetic fields show a clear metallic behavior between 10 and 400 K with a small anomaly (kink) near 321 K that corresponds to the ferrimagnetic ordering temperature of the material (Fig. 2). As the applied magnetic field increases, the resistance of the sample decreases at all temperatures but most significantly at temperatures below T_C. The magnitude of this magnetoresistive (MR) response is on the order of 30% to 40%, in good agreement with Maignan *et al.*'s reported results[2] obtained with their "metallic" Ba_2FeMoO_6 sample. It is important to note that this behavior is very different from that of Sr_2FeMoO_6 for which MR properties were observed only in nonmetallic samples.[3]

Interpreting the field-dependent resistance measurements, Maignan and his co-workers[2] suggested the MR behavior of Ba_2FeMoO_6 as due to spin-dependent carriers being transferred across the grain boundaries in the bulk. The same investigators also showed that modifying the properties of grain boundaries could be used to control this intergranular MR behavior. Indeed, a significant enhancement of the intergranular MR response from 20% to 37% (at 70 kOe) was obtained for a postannealed sample exhibiting semiconducting and metallic properties above and below T_C, respectively. At temperatures near T_C, however, the magnitude of the MR response remains unchanged, thus leading to the conclusion that intragranular MR bulk effects are also present. Further

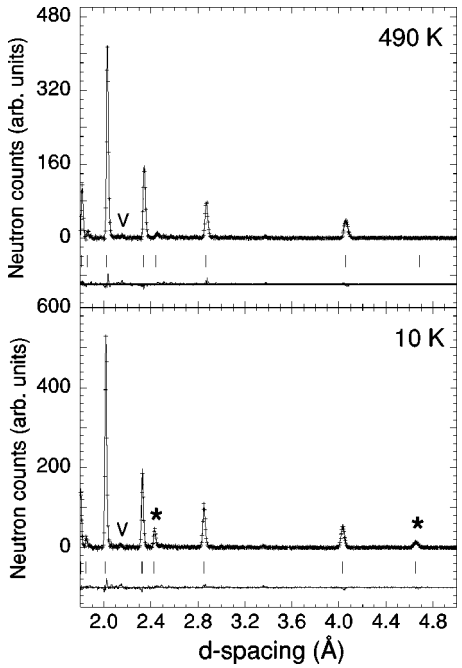

FIG. 3. Portions of the best-fit Rietveld profiles obtained using the tetragonal space group $I4/mmm$ at 10 K and the cubic space group $Fm\bar{3}m$ at 490 K. Observed (plus signs) and calculated (solid line) intensities are shown together with their difference (bottom). Bragg positions are indicated by the tick marks below the patterns. Asterisks indicate the locations of the observed main magnetic intensities modeled using the ferromagnetic space group $I4/mm'm'$. The letter V refers to the vanadium peak of the sample can holder.

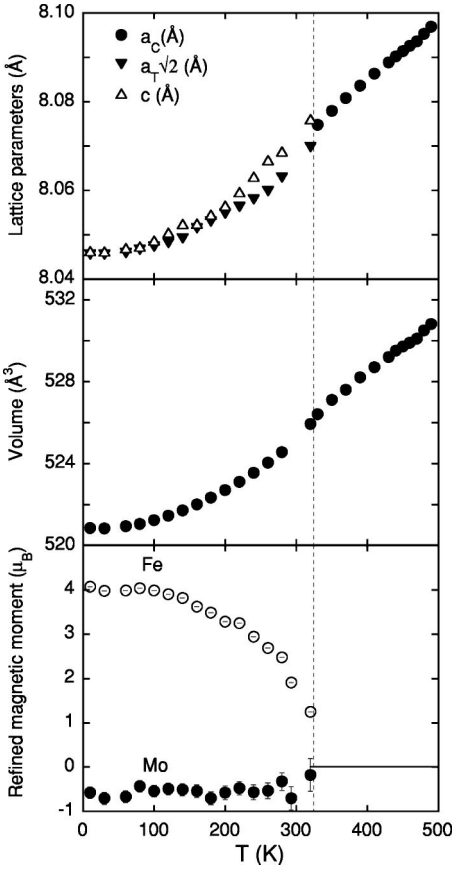

FIG. 4. The behavior of the lattice parameters (top panel) and unit cell volume (middle panel) as a function of temperature shows visible kinks near the ferrimagnetic transition temperature. The subscripts C and T refer to cubic and tetragonal, respectively. The difference between the tetragonal lattice parameters a and c is very subtle, indicating the pseudocubic nature of the structure. The refined magnetic moment of Fe and Mo (bottom panel) yield values of 4.1(1) and −0.58(1) μ_B, respectively, at 10 K with a ferrimagnetic moment of 3.52 μ_B, in good agreement with the magnetization's results (bottom panel). Dashed lines indicate the approximate location of the cubic-to-tetragonal phase transition.

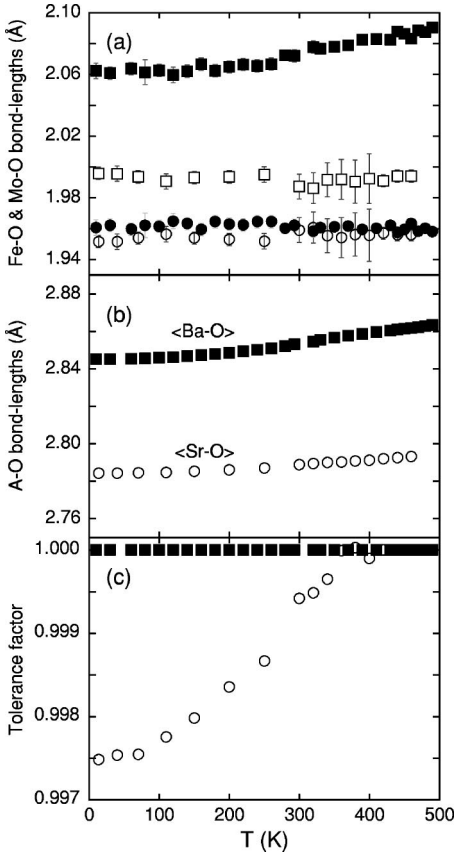

FIG. 5. (a) Average ⟨Fe—O⟩ (squares) and ⟨Mo—O⟩ (circles) bond lengths for Ba_2FeMoO_6 (filled symbols) and Sr_2FeMoO_6 (open symbols). (b) Average ⟨Ba—O⟩ and ⟨Sr—O⟩ bond lengths as a function of temperature. (c) Tolerance factor, calculated using our refined bond lengths, for Ba_2FeMoO_6 (filled squares) and Sr_2FeMoO_6 (open circles).

evidence for the intergranular MR behavior below T_C was presented by Yin *et al.*,[16] who measured the behavior of the resistance within the grain and across grain boundaries in a Sr_2FeMoO_6 thin film deposited on a $SrTiO_3$ bicrystal substrate.

Neutron powder diffraction

Neutron diffraction patterns reveal the presence of a trace amount (~1% by weight or less) of $BaMoO_4$ (tetragonal $I4_1/a$, $a=5.582$ and $c=12.82$ Å) as an impurity phase. The weight percentage of $BaMoO_4$ was estimated qualitatively from the very weak intensities of its barely visible Bragg peaks and from unsuccessful attempts to include and stabilize the refinements of the structural parameters of this phase. The presence of this phase implies, however, that other minute impurity phases might also be present. The presence of a very small amount of elemental Fe (cubic $Im\bar{3}m$, $a=2.852$ Å) is possible but could not be confirmed because of the accidental overlapping of its "expected" peaks, if any, at 2.03, 1.43, 1.17, and 1.01 Å with the main Ba_2FeMoO_6 peaks (namely, the cubic 400, 440, 444, and 800 lines, respectively). Small amounts of elemental Fe were seen, however, in other related materials, such as Sr_2FeMoO_6 and Ca_2FeMoO_6, samples prepared under similar synthesis conditions (data not shown). To explore the possible off-stoichiometry of the investigated sample, we refined the site occupancies for Fe, Mo, and O at all temperatures above T_C (twelve independent data sets) where the magnetic peaks are absent and cannot interfere with the refined occupancies (unit cells due to ferrimagnetic ordering and Fe/Mo cation ordering are the same). These refinements practically yielded constant values for the refined site occupancies and as such, the mean values $n_{(Fe)}=1.01(1)$, $n_{(Mo)}=0.96(1)$, and $n_{(O)}=1.005(10)$ were determined and kept fixed in all subsequent refinements at all temperatures. While Fe and O sites are essentially full, the Mo refined site occupancy indicates the possible presence of some vacancies on this site, in agreement with the presence of the $BaMoO_4$ impurity phase that could slightly offset the final composition of the main phase. Other studies proposed the substitution of Fe on the Mo sites in Sr_2FeMoO_6 or the presence of antisite defect patches[17,18]

TABLE I. Select structural parameters and bond-lengths for Ba_2FeMoO_6. Tetragonal atom positions are: Fe at (0 0 0), Mo at $(0\ 0\ \frac{1}{2})$, Ba at $(\frac{1}{2}\ 0\ \frac{1}{4})$, $O_{equatorial}$ at (x x 0) and O_{apical} at (0 0 z). Cubic atom positions are: Fe at (0 0 0), Mo at $(\frac{1}{2}\ \frac{1}{2}\ \frac{1}{2})$, Ba at $(\frac{1}{4}\ \frac{1}{4}\ \frac{1}{4})$, and O at (0 0 z). Fe and Mo magnetic moments were refined using the $I4/mm'm'$ magnetic symmetry (see text). U's are multiplied by a factor of 100.

T (K)	→	10	100	200	295	390	490
Atom	Variable	$I4/mmm$	$I4/mmm$	$I4/mmm$	$I4/mmm$	$Fm\bar{3}m$	$Fm\bar{3}m$
	a (Å)	5.68902(2)	5.69028(2)	5.69553(2)	5.70409(2)	8.08355(4)	8.09689(4)
	c (Å)	8.04621(5)	8.04867(5)	8.05648(5)	8.07014(5)		
	V (Å^3)	260.415(3)	260.610(3)	261.344(3)	262.575(3)	528.210(7)	530.828(7)
Fe	U_{iso} (Å^2)	0.26(6)	0.33(6)	0.35(6)	0.54(6)	0.61(4)	0.78(5)
	m (μ_B)	4.1(1)	4.0(1)	3.3(1)	1.9(2)		
Mo	U_{iso} (Å^2)	0.22(8)	0.27(9)	0.5(1)	0.46(9)	0.66(6)	0.63(6)
	m (μ_B)	−0.58(14)	−0.55(13)	−0.58(16)	−0.7(3)		
	$m_{Fe}-m_{Mo}$	3.5(1)	3.45(1)	2.72(1)	1.2(2)		
Ba	U_{iso} (Å^2)	0.14(2)	0.24(2)	0.38(2)	0.51(2)	0.80(2)	0.97(2)
$O_{equatorial}$	x	0.2546(6)	0.2537(5)	0.2538(5)	0.2542(4)		
	U_{11} (Å^2)	0.3(3)	0.4(2)	0.4(2)	0.6(2)		
	U_{33} (Å^2)	0.8(4)	0.8(4)	1.0(4)	1.4(3)		
	U_{12} (Å^2)	0.0(2)	−0.1(3)	−0.1(3)	−0.1(2)		
O_{apical}	z	0.2598(14)	0.2615(10)	0.2614(10)	0.2620(9)	0.2576(2)	0.2582(2)
(or O in cubic)	U_{11} (Å^2)	0.2(4)	0.3(3)	0.4(4)	0.4(3)	0.73(4)	0.81(5)
	U_{33} (Å^2)	0.7(4)	0.8(3)	0.9(3)	0.7(3)	1.052(2)	1.28(2)
R_P (%)		4.48	4.49	4.98	4.82	5.01	4.78
R_{WP} (%)		6.68	6.69	7.69	7.4	7.74	7.52
χ^2		1.377	1.365	1.486	1.390	1.335	1.309
$Fe-O_{ap.}$ (Å)	×2	2.090(11)	2.105(8)	2.106(8)	2.115(8)		
$Fe-O_{eq.}$ (Å)	×4	2.048(5)	2.041(4)	2.044(4)	2.051(4)		
⟨Fe–O⟩ (Å)	×6	2.0622	2.0625	2.0648	2.0720	2.082(2)	2.090(2)
$Mo-O_{ap.}$ (Å)	×2	1.933(11)	1.920(8)	1.922(8)	1.920(8)		
$Mo-O_{eq.}$ (Å)	×4	1.975(5)	1.982(4)	1.983(4)	1.983(4)		
⟨Mo–O⟩ (Å)	×6	1.9606	1.9614	1.9628	1.9620	1.959(2)	1.958(2)

that consist mostly of Fe rich clusters. Our results, however, can only be interpreted as due to Mo vacancies because Fe substitution on the Mo site would otherwise result in a Mo site occupancy being greater than unity (because of the larger scattering length of Fe). Indeed, attempts to perform such refinements resulted in meaningless occupancies.

The structure of Ba_2FeMoO_6 is cubic $Fm\bar{3}m$ at all temperatures above T_C, as shown in the best-fit Rietveld profile in Fig. 3. Within the resolution limits of our diffractometer, no sign of additional peaks or peak splitting has been observed, below T_C, in any of the data collected down to 10 K. However, taking into account the ferromagnetic ordering of the Fe and Mo sublattices and the observed increased intensities of a few Bragg peaks due to the ferrimagnetic structure, the actual symmetry of the material in its ferromagnetic state is required to be lower than cubic to create a unique magnetic axis.[19,20] Otherwise, in the cubic symmetry, the magnetic structure could not be introduced and refined. Thus, refinements were attempted with the symmetry lowered to that of tetragonal $I4/mmm$, which is a subgroup of $Fm\bar{3}m$. These refinements converged with a slight elongation of the c axis with respect to the basal a axis. In this tetragonal space group, ferromagnetically aligned spins can be introduced in the direction of the c axis by taking the time reversal symmetry of the m mirrors that are perpendicular to the ⟨100⟩ and ⟨110⟩ directions, thus, resulting in the tetragonal magnetic space group $I4/mm'm'$. In this space group, the Fe and Mo octahedra are no longer isotropic because the oxygen atoms surrounding Fe (or Mo) split into two apical and four equatorial atoms, thus, giving rise to independent bonds in the in-plane and apical directions. Refined structural parameters and bond lengths are listed in Table I.

Lattice parameters, unit cell volume, and refined magnetic moments for Fe and Mo are shown in Fig. 4 as a function of temperature. As shown in the figure, the ferrimagnetic ordering of the Fe and Mo moments clearly correlates with the

TABLE II. Bond-valence-sum (BVS) calculations, using room-temperature bond lengths, for Ba_2FeMoO_6, Sr_2FeMoO_6, and Ca_2FeMoO_6. BVS calculations were performed using the equation $v = \sum e^{(r_o - r_{ij})/B}$, where v is the calculated valence, $B = 0.37$ is an empirical universal constant, $r_o = 2.285$, 2.118, 1.967, 1.734, 1.759, 1.907, and 1.907 for Ba, Sr, Ca, Fe^{2+}, Fe^{3+}, Mo^{5+}, and Mo^{6+}, respectively, and r_{ij} represents the cation-to-anion bond lengths (see Refs. 22 and 25).

Bond-length (Å)	Ba_2FeMoO_6	Sr_2FeMoO_6	Ca_2FeMoO_6
$Fe-O_{ap.}$	$2.115(8)\times 2$	$1.996(15)\times 2$	$1.986(7)\times 2$
$Fe-O_{eq.}$	$2.051(4)\times 4$	$1.983(8)\times 4$	$2.016(5)\times 2$
$Fe-O_{eq.}$			$2.015(5)\times 2$
$Mo-O_{ap.}$	$1.920(8)\times 2$	$1.951(15)\times 2$	$1.977(7)\times 2$
$Mo-O_{eq.}$	$1.983(4)\times 4$	$1.963(8)\times 4$	$1.971(5)\times 2$
$Mo-O_{eq.}$			$1.966(5)\times 2$
$A-O_{ap.}$	$2.8537(3)\times 4$	$2.7866(1)\times 4$	$3.165(2)\times 1$
$A-O_{ap.}$			$2.446(2)\times 1$
$A-O_{ap.}$			$2.351(3)\times 1$
$A-O_{ap.}$			$3.117(3)\times 1$
$A-O_{eq.}$	$2.85284(4)\times 8$	$2.711(3)\times 4$	$2.626(9)\times 1$
$A-O_{eq.}$		$2.869(3)\times 4$	$2.368(10)\times 1$
$A-O_{eq.}$			$3.362(10)\times 1$
$A-O_{eq.}$			$2.689(11)\times 1$
$A-O_{eq.}$			$2.615(9)\times 1$
$A-O_{eq.}$			$2.368(10)\times 1$
$A-O_{eq.}$			$3.361(10)\times 1$
$A-O_{eq.}$			$2.692(10)\times 1$
	$v_{Ba}=2.58$	$v_{Sr}=1.96$	$v_{Ca}=2.06$
Using r_o for Fe^{2+}	$v_{Fe}=2.41$	$v_{Fe}=3.03$	$v_{Fe}=2.89$
Using r_o for Fe^{3+}	$v_{Fe}=2.58$	$v_{Fe}=3.23$	$v_{Fe}=3.08$
Using r_o for Mo^{5+}	$v_{Mo}=4.80$	$v_{Mo}=4.82$	$v_{Mo}=5.04$
Using r_o for Mo^{6+}	$v_{Mo}=5.19$	$v_{Mo}=5.21$	$v_{Mo}=5.04$

behavior of the unit cell lattice parameters and volume. At 10 K, Fe and Mo moments refined to $\sim 4.1(1)\ \mu_B$ and $\sim -0.58(1)\ \mu_B$, respectively, with a net ferrimagnetic moment of $\sim 3.52\ \mu_B$, in good agreement with the magnetization data shown in Fig. 1 and other similar values reported in the literature. The practically constant Mo moment refined to a value of $\sim -0.58(1)\ \mu_B$ at most temperatures below T_C, which is significantly lower than the theoretical value of $-1\ \mu_B$ expected for Mo^{5+} ions but is in agreement with several studies showing the itinerant character of the $Mo_{t_{2g}}\downarrow$ electron that is shared between Mo and Fe. Similarly, the value of 4.1 μ_B for Fe is significantly lower than the value of 5 μ_B that would be expected for Fe^{3+} ions. As explained above, reduction of the refined Fe moment could be attributed to the presence of Fe and Mo ions in different oxidation states (Fe^{2+}/Fe^{3+} and Mo^{6+}/Mo^{5+}) as well as to vacancies and disrupted grain surface and boundaries.

Behavior of the average ⟨Fe—O⟩, ⟨Mo—O⟩, ⟨Ba—O⟩, and ⟨Sr—O⟩ bond lengths as a function of temperature is displayed in Fig. 5 for both Ba_2FeMoO_6 and Sr_2FeMoO_6 (data extracted from previous work[3]). As shown in the figure, the calculated average ⟨Mo—O⟩ bond lengths appear to be constant, and temperature and sample independent; however, a significantly larger ⟨Fe—O⟩ bond length is observed at all temperatures when compared to the corresponding bonds in Sr_2FeMoO_6 and Ca_2FeMoO_6. For example, an average room-temperature ⟨Fe—O⟩ bond length of ~2.075, 1.990, and 2.00 Å is observed for Ba_2FeMoO_6, Sr_2FeMoO_6, and Ca_2FeMoO_6 (data not shown),[21] respectively. On the other hand, the dependence of ⟨Fe—O⟩ bond length on temperature shows different behavior in Ba_2FeMoO_6 when compared to Sr_2FeMoO_6. In Sr_2FeMoO_6, an essentially constant ⟨Fe—O⟩ bond length is observed as a function of temperature, but in the case of Ba_2FeMoO_6, this bond is nearly constant only below ~200 K; it then increases monotonically at a rate of $\sim 8.93\times 10^{-5}$ Å/K between 200 and 490 K. In Sr_2FeMoO_6, the nuclear and magnetic structural phase transitions as well as the rotation of FeO_6 and MoO_6 octahedra appear to occur in the vicinity of T_C, thus making it difficult to firmly separate the steric effects due to pure geometrical considerations from the electronic effects that result from magnetic ordering (e.g., splitting of the *d* energy levels). As noted in our previous paper,[3] Fe—O bonds in Sr_2FeMoO_6 are relatively short and are essentially constant over a wide temperature range and the planar Fe—O and Mo—O bonds contract at a rate faster than the average thermal contraction, while the apical bonds contract at a slower rate. As the coordinated rotations of the corner-linked FeO_6 and MoO_6 octahedra grow, the different contraction rates allow the planar

and apical Fe—O and Mo—O bonds to maintain nominally constant lengths in spite of the thermal contraction. Thus, rotation of the FeO_6 octahedra occurs to relieve the internal geometrical strains caused by the Fe—O bonds being at or near their minimal sustainable value, the onset of this rotation does not have to coincide with the nuclear and/or magnetic structural transitions. As such, rotation of FeO_6 octahedra is not necessary in Ba_2FeMoO_6 because the $\langle$Fe—O$\rangle$ bonds are considerably larger (2.06 to 2.09 Å) than the suggested minimal value of ~1.98 Å. On the other hand, enhanced geometrical frustrations due to smaller *A*-site ions lead to larger structural distortions and to more degrees of freedom (octahedral rotations and tilts) being added to the system as demonstrated by the monoclinic $P2_1/n$ structural distortion of Ca_2FeMoO_6, for example, as reported by Ritter *et al.*[8] and others.[6,7]

Finally, we used the bond-valence sum method[22] to estimate the room-temperature oxidation states of Fe and Mo in Ba_2FeMoO_6, Sr_2FeMoO_6, and Ca_2FeMoO_6. As shown in Table II, the calculated valence states of Fe, Mo, Sr, and Ca ions (in Sr_2FeMoO_6 and Ca_2FeMoO_6) are in good agreement with their expected values based on the assumption of Fe^{3+}—Mo^{5+} pairs in the materials, however, significantly different values are obtained in the case of Ba_2FeMoO_6 with the oxidation states of Fe, Mo, and Ba calculated as ~(2.4–2.5)+, ~(4.8–5.2)+, and ~2.58+, respectively, (see Table II for more details). The large oxidation state calculated for bivalent Ba is of particular interest because it indicates the presence of considerable strains within the structure in agreement with predictions based on the tolerance factor, calculated using nominal ionic sizes as tabulated in Shannon's paper,[23] suggesting that the synthesis of this material would be difficult under normal conditions. However, the tolerance factor (t), calculated using bond lengths extracted from our refinements, was found to be constant with $t=1.0$ at all temperatures between 10 and 490 K, thus indicating the cubic and pseudocubic nature of its structure even in its ferrimagnetic state and implying the presence of large strains between the different layers. Figure 5 also displays the temperature-dependent tolerance factor calculated for Sr_2FeMoO_6 that shows a normal behavior with the tolerance factor increasing with increased temperatures and then becoming constant ($t=1.0$) at all temperatures above the tetragonal/cubic phase transition.[24] The unusually large valence state calculated for Ba and the calculated tolerance factor imply that this ion is under compressive strains. Interpreting the results obtained for Fe and Mo, on the other hand, is not straightforward because of their multiple oxidation states and the itinerant nature of the $Mo_{t_{2g}}$ electrons, however, we speculate that Fe and Mo layers must be experiencing tensile strains to at least partially counterbalance the compressive strains in the Ba layers. More investigative work is needed to resolve this issue.

CONCLUSIONS

Using neutron powder diffraction, we have investigated the evolution of the nuclear and magnetic structures of Ba_2FeMoO_6 as a function of temperature. The lattice parameters and unit cell volume of Ba_2FeMoO_6 are considerably larger than those of Sr_2FeMoO_6. Similar to Sr_2FeMoO_6, the structure of Ba_2FeMoO_6 undergoes a phase transition from cubic $Fm\bar{3}m$ to tetragonal (pseudocubic) $I4/mmm$ at T_C but, unlike Sr_2FeMoO_6, the FeO_6 and MoO_6 octahedra do not exhibit any rotations. The cubic to tetragonal structural transition is required by the ferrimagnetic interaction of the Fe and Mo spins with the nuclear lattice. The ferrimagnetic structure of Ba_2FeMoO_6 can be described using the symmetry of the tetragonal magnetic $I4/mm'm'$ space group. Finally, our refinements show that the Fe and Mo moments are considerably lower and larger than their expected values in Fe^{3+}—Mo^{5+} and Fe^{2+}—Mo^{6+}, respectively, thus suggesting the presence of a mixture of both combinations. Bond-valence-sum calculations show the presence of significant strains in the system due to the large size of the Ba ions.

ACKNOWLEDGMENTS

Work at NIU was supported by the NSF, Grant No. DMR-0302617, and by the State of Illinois under HECA. At ANL, this work was supported by the U.S. Department of Energy, Division of Basic Energy Science-Materials Sciences, under Contract No. W-31-109-ENG-38 (the operation of IPNS).

[1] K.-I. Kobayashi, T. Kimura, H. Sawada, K. Terakura, and Y. Tokura, Nature (London) **395**, 677 (1998).
[2] A. Maignan, B. Raveau, C. Martin, and M. Hervieu, J. Solid State Chem. **144**, 224 (1999).
[3] O. Chmaissem, R. Kruk, B. Dabrowski, D. E. Brown, X. Xiong, S. Kolesnik, J. D. Jorgensen, and C. W. Kimball, Phys. Rev. B **62**, 14197 (2000).
[4] Y. Moritomo, S. Xu, A. Machida, T. Akimoto, E. Nishibori, M. Takata, M. Sakata, and K. Ohoyama, J. Phys. Soc. Jpn. **69**, 1723 (2000).
[5] N. Nguyen, F. Sriti, C. Martin, F. Bouree, J. M. Greneche, A. Ducouret, F. Studer, and B. Raveau, J. Phys.: Condens. Matter **14**, 12629 (2002).
[6] L. Pinsard-Gaudart, R. Surynarayanan, A. Revcolevschi, J. Rodriguez-Carvajal, J.-M. Greneche, P. A. I. Smith, R. M. Thomas, R. P. Borges, and J. M. D. Coey, J. Appl. Phys. **87**, 7118 (2000).
[7] J. A. Alonso, M. T. Casais, M. J. Martínez-Lope, J. L. Martínez, P. Velasco, A. Muñoz, and M. T. Fernández-Díaz, Chem. Mater. **12**, 161 (2000).
[8] C. Ritter, M. R. Ibarra, L. Morellon, J. Blasco, J. Garcia, and J. M. Teresa, J. Phys.: Condens. Matter **12**, 8295 (2000).
[9] M. Besse *et al.*, Europhys. Lett. **60**, 608 (2002).
[10] J. M. Greneche, M. Venkatesan, R. Suryanarayanan, and J. M. D. Coey, Phys. Rev. B **63**, 174403 (2001).
[11] J.-S. Kang *et al.*, Phys. Rev. B **66**, 113105 (2002).

[12] X. M. Feng, G. H. Rao, G. Y. Liu, Z. W. Ouyang, and J. K. Liang, J. Phys.: Condens. Matter **16**, 1813 (2004).
[13] Y. Yasukawa, J. Lindén, T. S. Chan, R. S. Liu, H. Yamauchi, and M. Karppinen, Solid State Commun. **177**, 2655 (2004).
[14] J. D. Jorgensen, J. J. Faber, J. M. Carpenter, R. K. Crawford, J. R. Haumann, R. L. Hitterman, R. Kleb, G. E. Ostrowski, F. J. Rotella, and T. G. Worlton, J. Appl. Crystallogr. **22**, 321 (1989).
[15] A. C. Larson and R. B. von Dreele, General Structure Analysis System, University of California, 1985–1990.
[16] H. Q. Yin, J.-S. Zhou, J.-P. Zhou, R. Dass, J. T. McDevitt, and J. B. Goodenough, Appl. Phys. Lett. **75**, 2812 (1999).
[17] D. Sanchez, J. A. Alonso, M. Garcia-Hernandez, M. J. Martinez-Lope, M. T. Casais, and J. L. Martinez, J. Mater. Chem. **13**, 1771 (2003).
[18] D. Sanchez, J. A. Alonso, M. Garcia-Hernandez, M. J. Martinez-Lope, J. L. Martinez, and A. Mellergard, Phys. Rev. B **65**, 104426 (2002).
[19] W. Opechowski, *Crystallographic and Metacrystallographic Groups* (North-Holland, Amsterdam, 1986), Chap. 17, p. 474.
[20] W. Opechowski and R. Guccione, in *Magnetism*, edited by G. T. Rado (Academic, New York, 1965), Vol. II A, Chap. 3, p. 105.
[21] The structure of our Ca_2FeMoO_6 sample was refined using the symmetry of space group $P2_1/n$. Lattice parameters refined to $a=5.418\,35(6)$ Å, $b=5.524\,53(6)$ Å, $c=7.716\,84(8)$ Å, and $\beta=89.978(6)°$.
[22] I. D. Brown and D. Altermatt, Acta Crystallogr., Sect. B: Struct. Sci. **41**, 244 (1985).
[23] R. D. Shannon, Acta Crystallogr., Sect. A: Cryst. Phys., Diffr., Theor. Gen. Crystallogr. **32**, 751 (1976).
[24] B. Dabrowski, O. Chmaissem, J. Mais, S. Kolesnik, J. D. Jorgensen, and S. Short, Solid State Commun. **170**, 154 (2003).
[25] W. T. Liu and H. H. Thorp, Inorg. Chem. **32**, 4102 (1993).